CHAPTER III

STRUCTURAL ANALYSIS

The identification of grey tin, which is grown by LPE technique on InSb (111)B face is very difficult because the lattice constant of grey tin (6.478 Å) is very closed to the lattice constant of InSb (6.489 Å). In this thesis, the Electron Probe Microanalyzer (EPMA), and the x-ray back reflection technique were used to confirm grey tin on InSb. The first one will investigate Sn on InSb, and the second one will confirm the structure of Sn (grey or white phase). In this chapter will consider in detail about scanning electron microscopy (SEM) and x-ray microanalysis, and x-ray back reflection to follow the phase change of grey tin.

Scanning Electron Microscopy and X-Ray Microanalysis.(29)

The scanning electron microscope (SEM) is a powerful instrument which permits the observation and characterization of the semiconducting epitaxial surfaces or cross sections. The information on the film's microstructure obtained by the SEM investigation, can contribute to a better understanding of some properties of semiconducting thin films. In this instrument, the area to be examined or the microvolume with a finally focused electron beam, which is swept in a raster across the surface of the specimen. The types of interested signals produced when the electron beam impinges

on a specimen surface include mainly the secondary electron and back scattered electrons. The signals can be used to examine many characteristics of the sample such as surface topography, crystallography, etc. As the signals vary when the electron beam sweeps across different surface topography of the specimen, the secondary electron emission permits image of a volume near the impact area to be obtained at relative high resolution. The back scattered electrons and the large depth of field of the SEM help to create the three dimensional appearances of the images. SEM micrographs generally give features of the specimen image in three dimension at high magnification which cannot be given by ordinary optical microscopes.

The versatility of the SEM for the study of solids is derived in large measure from the rich variety of interactions which the beam electrons undergo within the specimen. The interactions can be generally divided into two classes : 1) elastic events, which effect the trajectories of the beam electrons within the specimen without significantly altering the energy, and 2) inelastic events, which result in a transfer of energy to the solid, leading to the generation of secondary electrons, Auger electrons, characteristic and continuum x-rays, long- wavelength electromagnetic radiation in the visible, ultraviolet, and infrared regions, electron-hole pairs, lattice vibrations (phonons), and electron oscillations (plasmons). In principle, all of these interactions can be used to derive information about the nature of the specimen : shape, composition, crystal structure, internal electric or magnetic fields, etc.

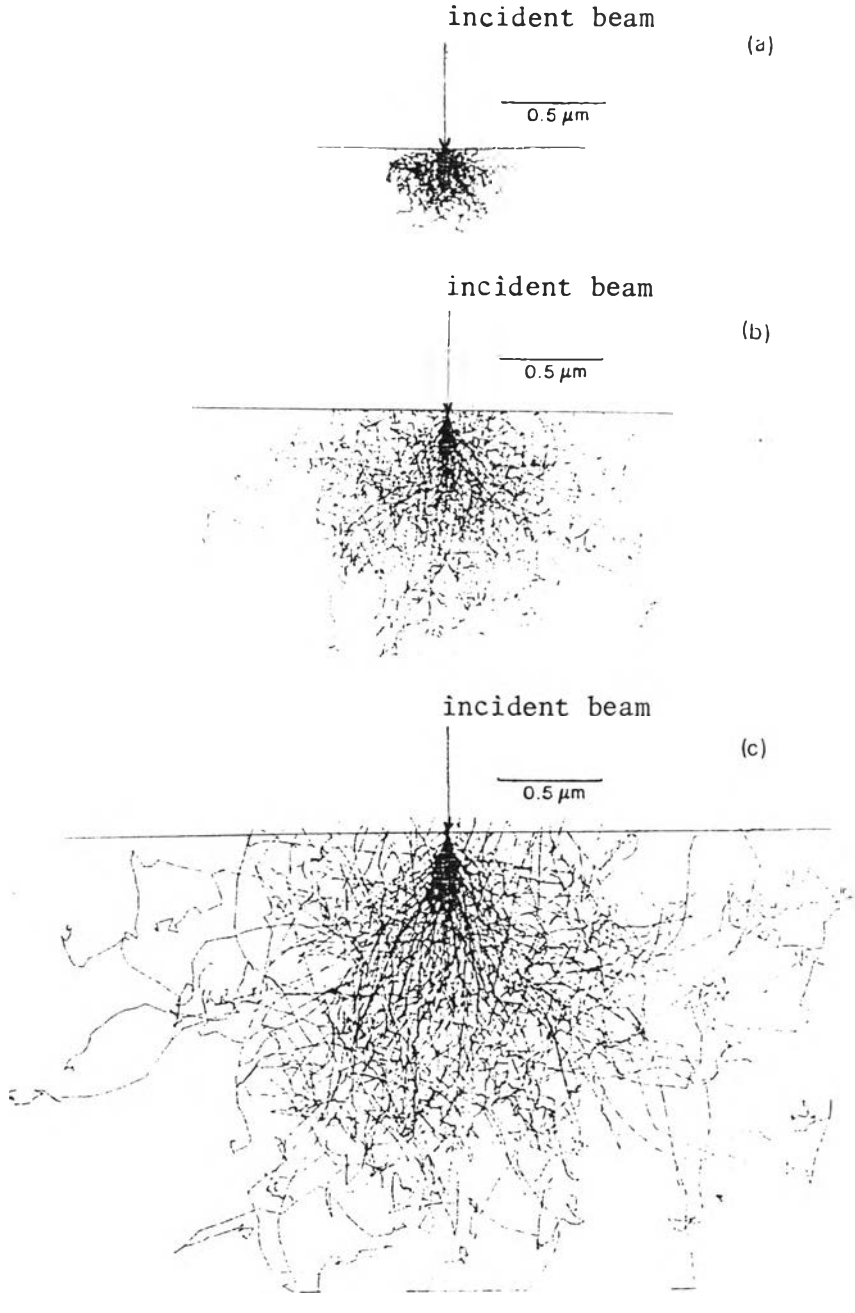

Fig.21 Monte Carlo calculations of the interaction volume in iron as a function of beam energy: (a) 10keV, (b) 20keV, (c) 30keV,

The region over which the beam electrons interact with the solid, depositing energy and producing those forms of secondary radiation which we measure, is known as the interaction volume. An understanding of the size and shape of the interaction volume as a function specimen and beam parameters is vital to proper interpretation of SEM images and microanalysis. The size of the interaction is a strong function of the energy with which the beam electrons interact with the sample : the increase in size with beam energy. The cross section for elastic scattering of electrons has an inverse dependence on the square of the energy. Thus, as the energy increase, the electron trajectories near the surface become straighter and the electrons penetrate more deeply into the solid before the effects of multiple scattering cause some of the electrons to propagate back toward the surface. At higher energy, the electrons can penetrate to greater depths since they retain a larger fraction of their initial energy after a given length of travel. The interaction volume as a function of beam energy as shown in the Monte Carlo plots of Fig. 21. Note that the shape of interaction volume does not change or significantly with a change in beam energy.

1. X-Ray Production.

During inelastic scattering of the beam electrons, x-rays can be formed by two distinctly different processes : 1) Deceleration of the beam electron in the Coulomb field of the atom core, which consists of the nucleus and tightly bound electrons, leads to formation of a continuous spectrum of x-ray energies from zero energy up to the value of the incident electron energy. This is referred to

as the x-ray continuum or bremsstrahlung ("braking radiation"). 2) The interaction of a beam electron with an inner-shell electron can result in the ejection of the bound electron which leaves the atom in an excited state with a vacancy in the electron shell. During subsequent deexcitation, an electron transition occurs from an outer shell to fill this vacancy. The transition involves a change in energy, and the energy released from the atom manifest itself either in the form of an x-ray or an ejected (Auger) electron. Since the energy of the emitted x-ray is related to the difference in energy between the sharply defined levels of the atom, it is referred to as a characteristic x-ray.

If the energy of the characteristic radiation from element A exceeds the absorption energy for element B in a sample containing A and B, then characteristic fluorescence of B by A will occur. To examine this situation, consider a sample containing indium, tin, and antimony which correspond to this experiment : epitaxial Sn on InSb. Table 3 (30) showed the L series x-ray wavelengths and energies. The absorption energy for indium is lower than the $L\alpha_1$ energies for tin and antimony, therefore characteristic fluorescence will occur from these radiations. The arguments can be repeated for each element in the specimen as shown in Table 4.

Table 3 L Series X-Ray Wavelengths and Energies

Element	$L\alpha_1$		$L\beta_1$	
	(Å)	E(keV)	(Å)	E(keV)
49 In	3.772	3.287	3.556	3.487
50 Sn	3.600	3.444	3.386	3.662
51 Sb	3.439	3.605	3.224	3.843

Table 4 Fluorescence in a sample containing In, Sn, and Sb

Element	Radiation causing fluorescence
In	(Sn $L\alpha_1$, $L\beta_1$; Sb $L\alpha_1$, $L\beta_1$)
Sn	(Sb $L\alpha_1$, $L\beta_1$)
Sb	None

2. X-Ray Spectral Measurement : WDS and EDS.

Chemical analysis in scanning electron microscope and electron microprobe is performed by measuring the energy and intensity distribution of the x-ray signal generated by a focused electron beam. The subject of x-ray production has already been introduced in the section 1) which describes the mechanisms for both characteristic and continuum x-ray production. This section is concerned with the methods for detecting and measuring these signals as well as converting them into a useful form for qualitative and quantitative analysis.

2.1 Wavelength-Dispersive Spectrometer (WDS).

When solid state detectors were interfaced to micro-analyzer, the wavelength-dispersive spectrometer (WDS) was used almost exclusively for x-ray spectral characterization. The basic components of the WDS are illustrated in Fig. 22 A small portion of the x-ray signal generated from the specimen passes out of the electron optical chamber and impinges on an analyzing crystal. If Bragg's law is satisfied,

$$n\lambda = 2d \sin\theta \qquad (3.1)$$

(where n is an integer, 1, 2, 3,...; λ is the x-ray wavelength; d is the interplanar spacing of the crystal; and θ is the angle of incidence of the x-ray on the crystal), the x-rays will be diffracted and detected by a proportional counter. The signal from the detector is amplified, converted to a standard pulse size by a single-channel analyzer (SCA) and then either counted with a scaler or displayed as a rate meter (RM) output on a strip chard recorder. A qualitative analysis therefore involves obtaining a strip chart recording of x-ray intensity as a function of crystal angle, converting peak positions to wavelengths through Bragg's law, and then using the Moseley relationship,

$$\lambda = B/(Z - C)^2 \qquad (3.2)$$

(where B and C are constants which differ for each family of spectral lines, λ is the characteristic x-ray wavelength, and Z is the atomic

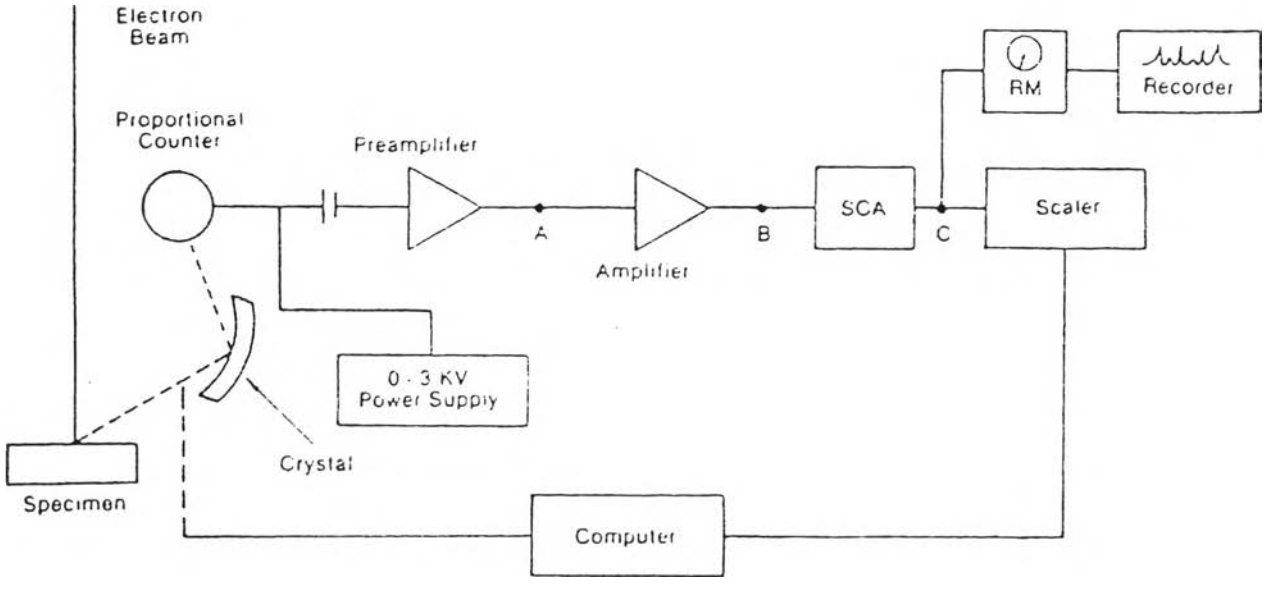

Fig.22 Schematic representation of a wavelength-dispersive spectrometer.

number) to relate the detected wavelengths to the presence of specific elements. In practice, crystal spectrometer readings are either proportional to wavelength or calibrated directly in wavelength. Standard tables can then be used for elemental identification.

The identification of the elements present in selected areas of the Sn on InSb sample were shown in Fig. 23, where a part of the x-ray spectrum from Sn on InSb is. SEM with 2 Channel Wavelength Dispersive X-Ray Spectrometer JEOL Model JSM-35CF was used in this thesis. The energy of the electron beam has to be selected to give a compromise between the requirements of resolution and x-ray production efficiency. On the one hand, a low overvoltage ratio U (ratio of beam energy to x-ray excitation energy) may be required to reduce electron penetration through the epitaxial Sn to the substrate InSb, in order to achieve a good spatial resolution; on the other hand, a relative high overvoltage ratio may be required to optimize the rate of x-ray production. For a thin film on a substrate (Sn on InSb), the situation which exists for x-ray generation is illustrated in Fig. 24. Electrons may generate x-ray in the film 1) directly or 2) after backscattering from the substrate. Electrons may backscatter from the film, transmit through the film, and backscatter from the substrate. Electrons may cross the film/substrate interface repeatedly before losing all their energy. In analysing Sn on InSb, the difficulty occurred because the atomic number of In, Sn, and Sb are 49, 50 and 51 respectively. The characteristic x-rays from K-shell of these elements cannot be seperated by WDS. We must use the characteristic x-rays from L-shell as shown in Fig. 23. However, if

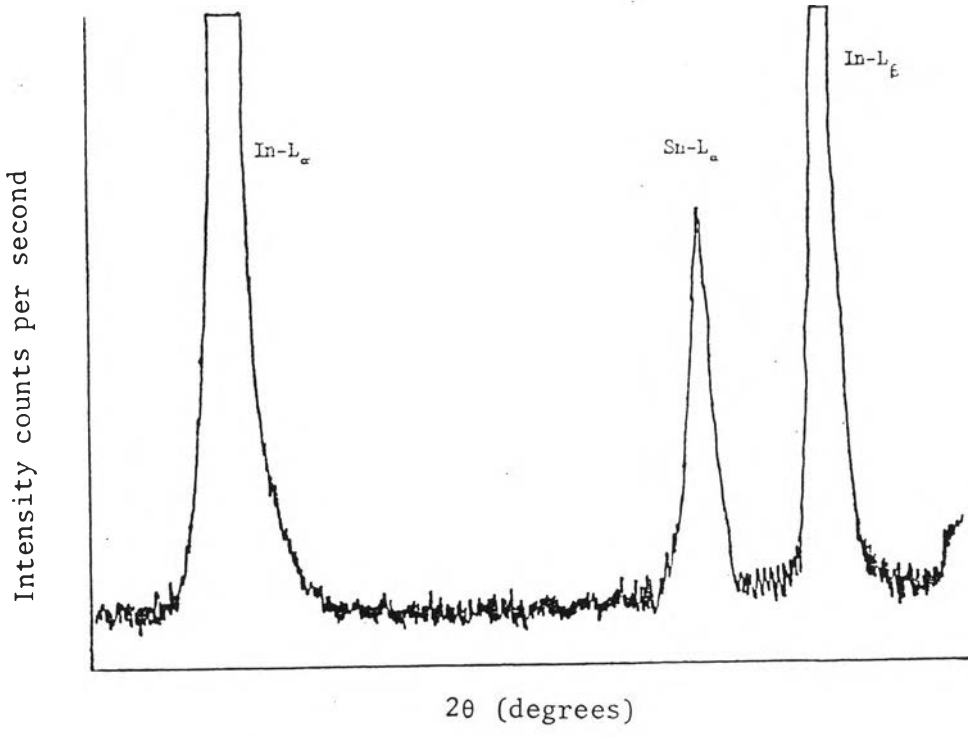

Fig.23 Part of x-ray spectrum of Sn on InSb.

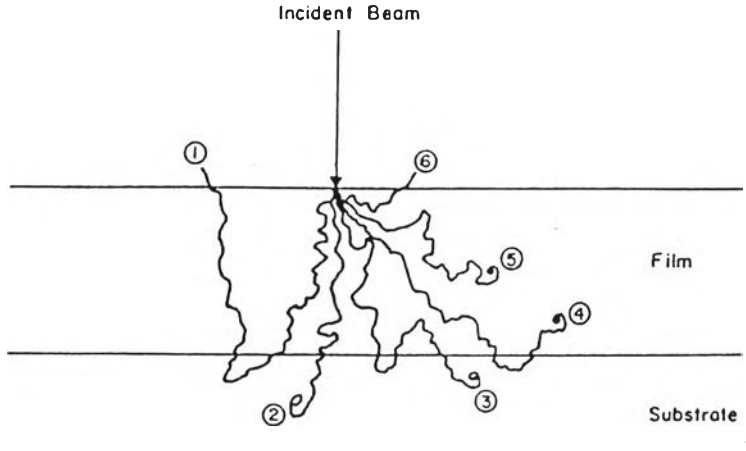

Fig.24 Examples of possible electron paths in a thin film on a substrate, Paths 1 and 6 lead to backscattering, while paths 2-5 remain in the film or substrate.

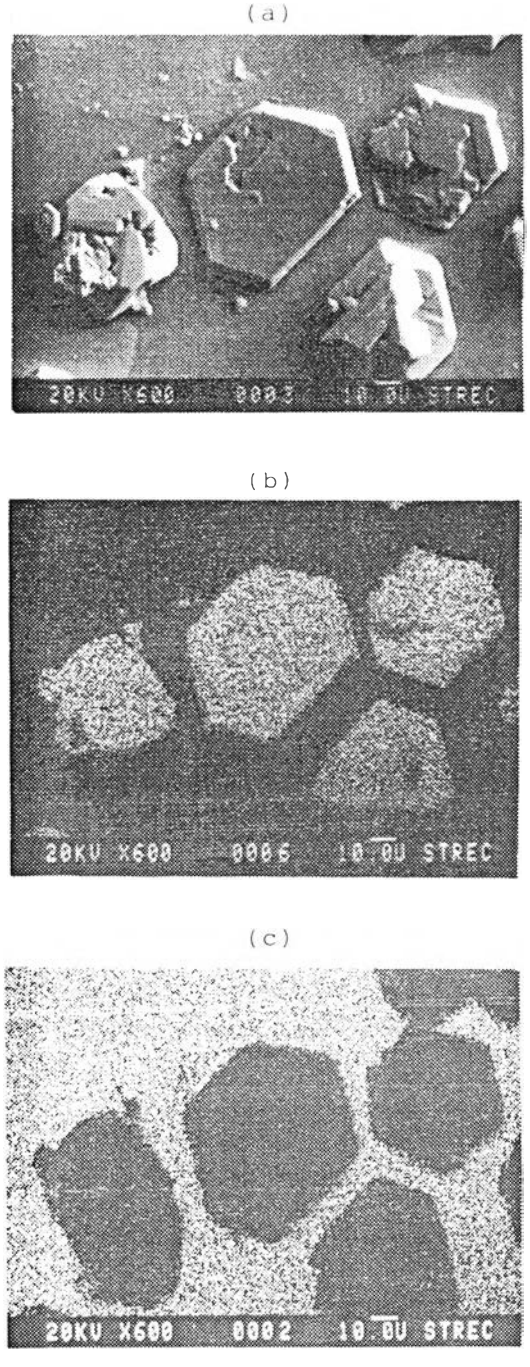

Fig. 25 The scanning electron image of planar sample Sn/InSb in (a), Sn mapping image in (b), and In mapping image in (c).

the Sn film is too thin in some samples, the electron beam energy must be decreased from 20 kV to 15 kV.

Two-dimensional scanning known as x-ray mapping involves taking the output of the SCA and using it to modulate the brightness of the CRT during normal secondary- electron raster scanning. Each x-ray photon detected appears as a dot on the CRT with regions of high concentration characterized by a high dot density. The x-ray mapping of In and Sn of the Sn on InSb sample showed in Fig. 25.

2.2 Energy-Dispersive X-Ray Spectrometer (EDS).

The operating principles of the solid state detectors are illustrated in Fig. 26. The x-ray signal from the sample passes through a thin beryllium window into a cooled, reversed-bias p-i-n (p-type, intrinsic, n-type) lithium- drifted silicon detector. Absorption of each individual x-ray photon leads to the ejection of a photoelectron which give up most of its energy to the formation of electron-hole pairs. They in turn are swept away by the applied bias to form a charge pulse by a charge-sensitive preamplifier. The signal is further amplified and shaped by a main amplifier and finally passed to a multichannel analyzer (MCA), where the pulses are sorted by voltage. The voltage distribution can be displayed on a cathode ray tube or an X-Y recorder.

For EDS, the resolution may be limited by defects and impurities in the Si detector, as well as the thermal and electrical

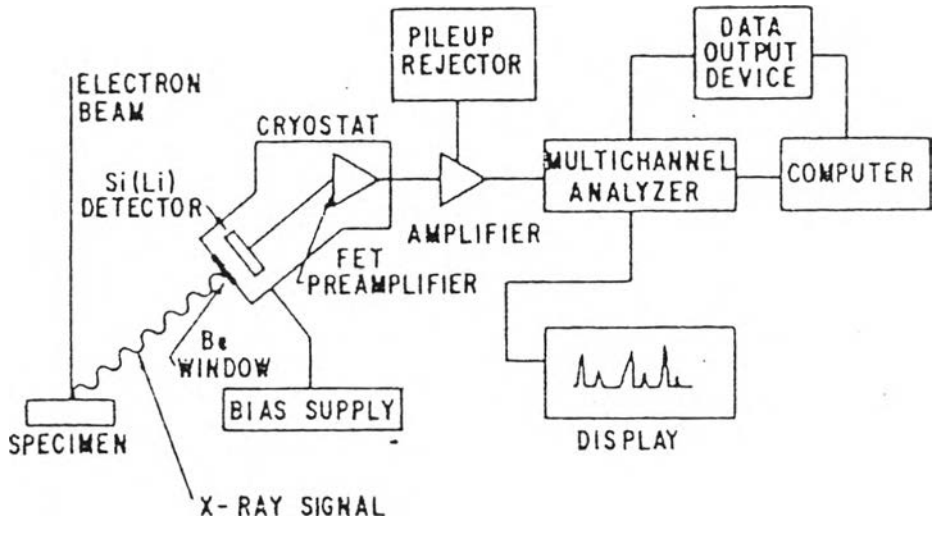

Fig.26 Schematic representation of an energy-dispersive spectrometer.

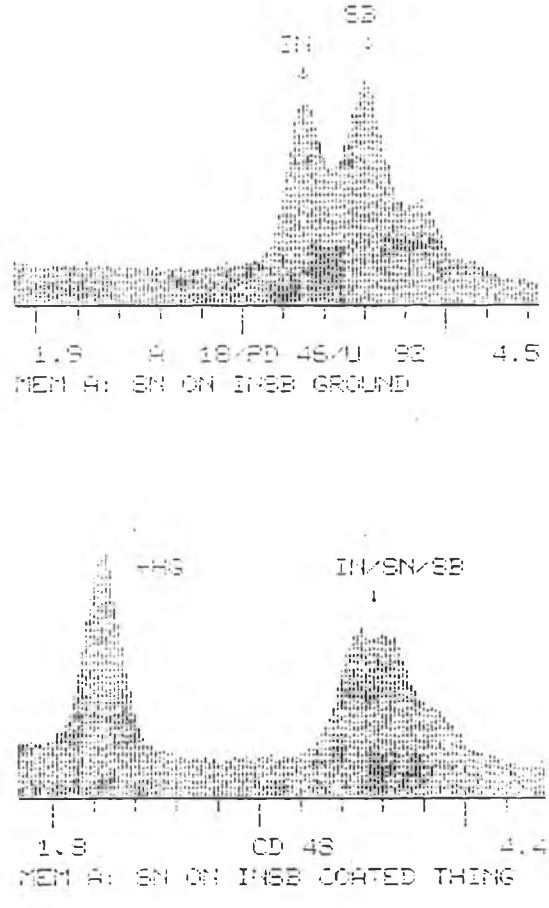

Fig.27 EDS spectrum of Sn on InSb, energy 15keV.

noise of the amplifiers. In qualitative analysis, thin film Sn on InSb, where the identification of low-intensity peak (Sn) near high-intensity peaks (In and Sb) may be difficult. We must compare the In and Sb peaks by focusing electron beam on substrate InSb with the peaks by focusing electron beam on Sn thin film. EDS spectrum of Sn on InSb illustrated in Fig. 27.

3. Results and Discussion Based on Electron Probe Micro Analysis (EPMA)

The scanning electron microscope (SEM) affords a larger magnification factor than that possible with an optical microscope. We examine the islet growths to determine whether it is Sn, and whether the growth is epitaxial. The wavelength dispersive spectrometer (WDS) technique is used to detect the presence of Sn; all methods of epitaxy experiments described in Chapter II yield deposit, if any, that is identified as Sn. Using the EPMA technique along the path across the substrate-layer boundary (when the sample is cleaved to expose such boundary) can detect the presence of oxygen and thus can map such presence as a function of position. The presence of an oxide layer and its thickness can be photographed, leading to the hypothesis that epitaxial growth is through pin holes in the oxide layer.

The EPMA/WDS can map the presence of Sn, In and Sb individually to show that Sn is above InSb. The shape of the islands of Sn and the edges would identify whether the Sn growth is epitaxial to the InSb crystal orientation.

We now proceed to examine in details the experimental results. The order of presentation will be along the "methods" of epitaxy temperature-time profiles described in Chapter II.

Sample from "Method 1" (T = const., < T_s)

The results on sample 13, dipped at 10°C (3° below T_s) for 2 hours, are shown in Fig. 28. Evidently the islets tend to have the same edge orientation; a minority of them are not aligned with the majority. In c. the cleaved edge is shown. The presence of a "carpet" underneath the islets can be seen. EPMA/WDS shows that the carpet layer is 1 μ thick and contains oxygen, i.e. an oxide layer. Interestingly Fig. 28 d. depicts a matted, lower area on the left of the line; the right side is unetched. Here too the island growth protrude over the general etched area. Other frames in this Fig. 28 show interesting growth morphologies. A mis-oriented growth (non (111)) appears in frame (h).

Runs mode with "method 1" subsequence to the sample 13 experiment are in comparision with sample 13:-

Sample No.	T	t	Comments
13	10	2	no stirring
14	10.5	1	no stirring
15	9.5	2	1/2 stirring at 1 stop
16	10	2	continuous stirring

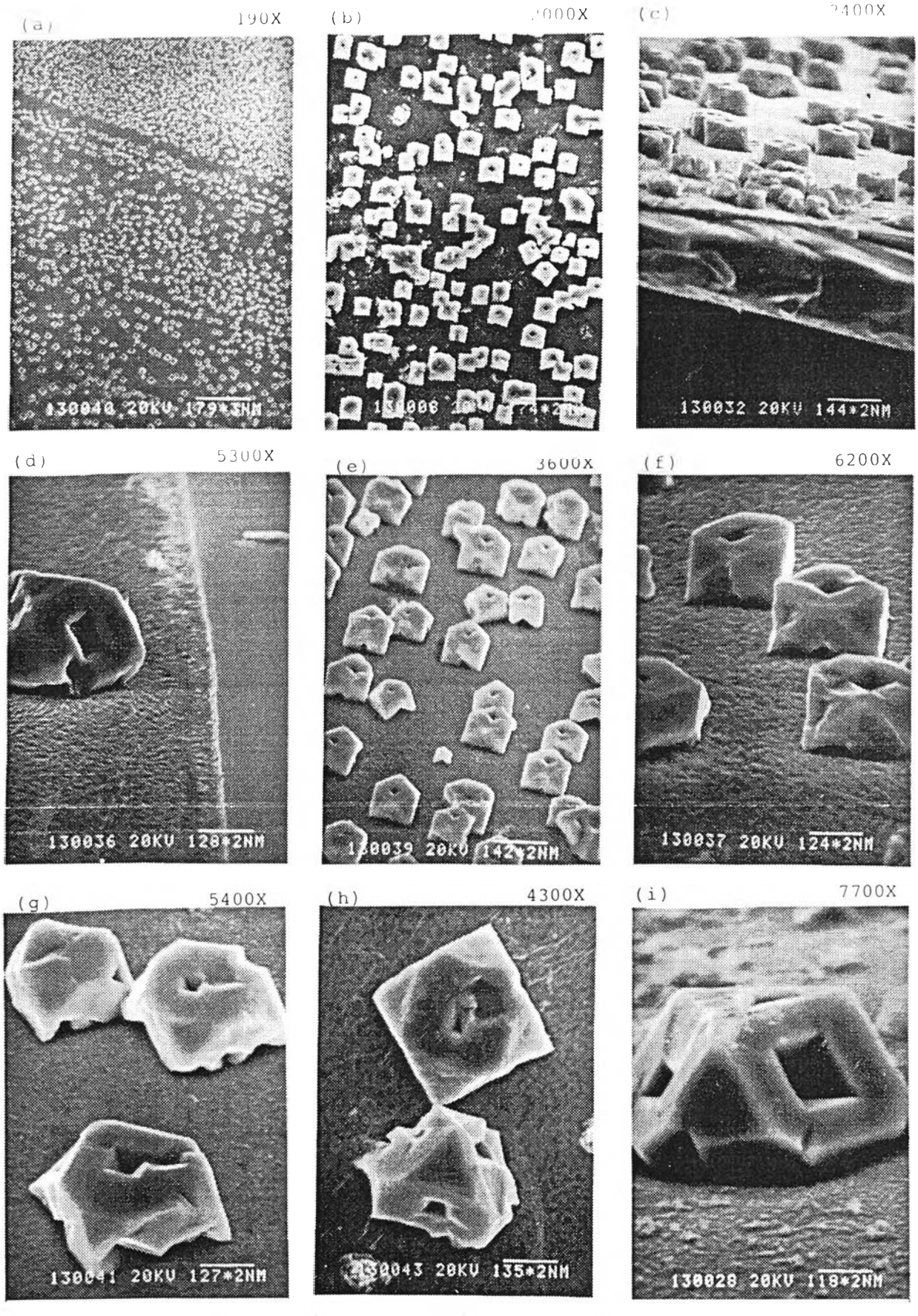

Fig.28 Scanning electron image at various magnifications at some areas show the islets of Sn and the etched surface of InSb of method (1) growth of sample no.13.

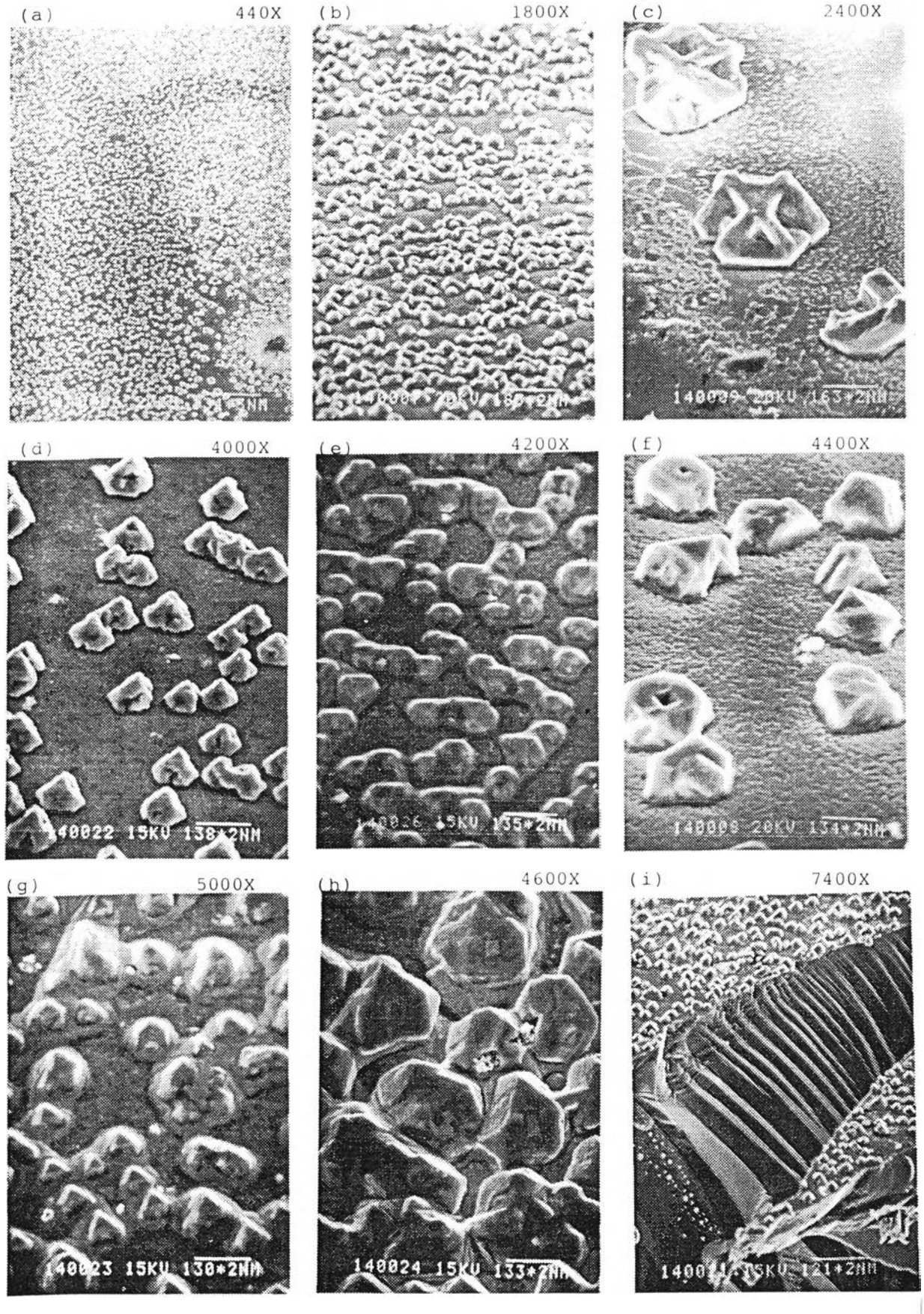

Fig.29 Scanning electron image at various magnifications at some areas show the islets of Sn and the etched surface of InSb of method (1) growth of sample no.11.

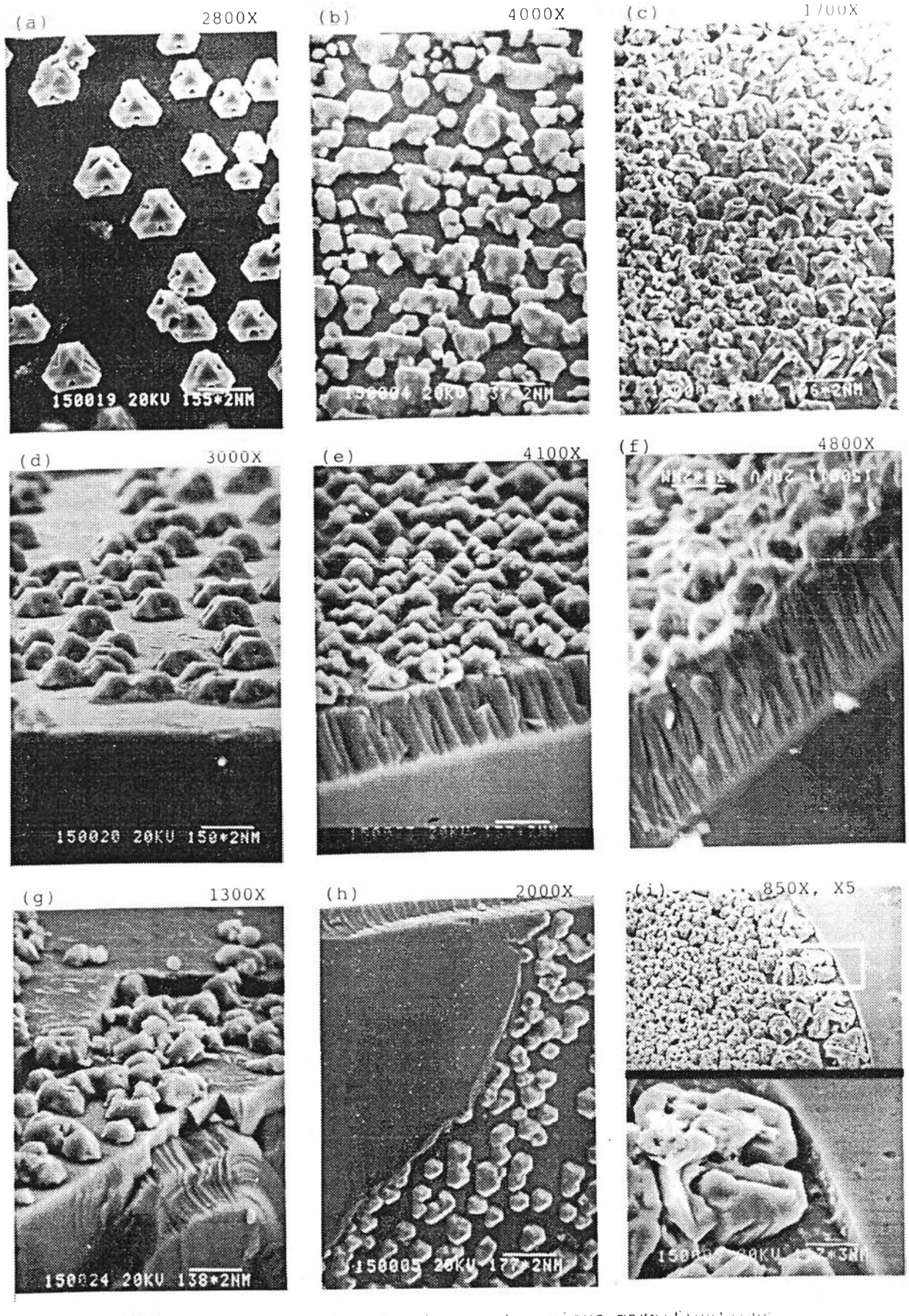

Fig.26 Scanning electron image at various magnifications at some areas show the islets of Sn and the etched surface of InSb of method 1) growth of sample no. 15.

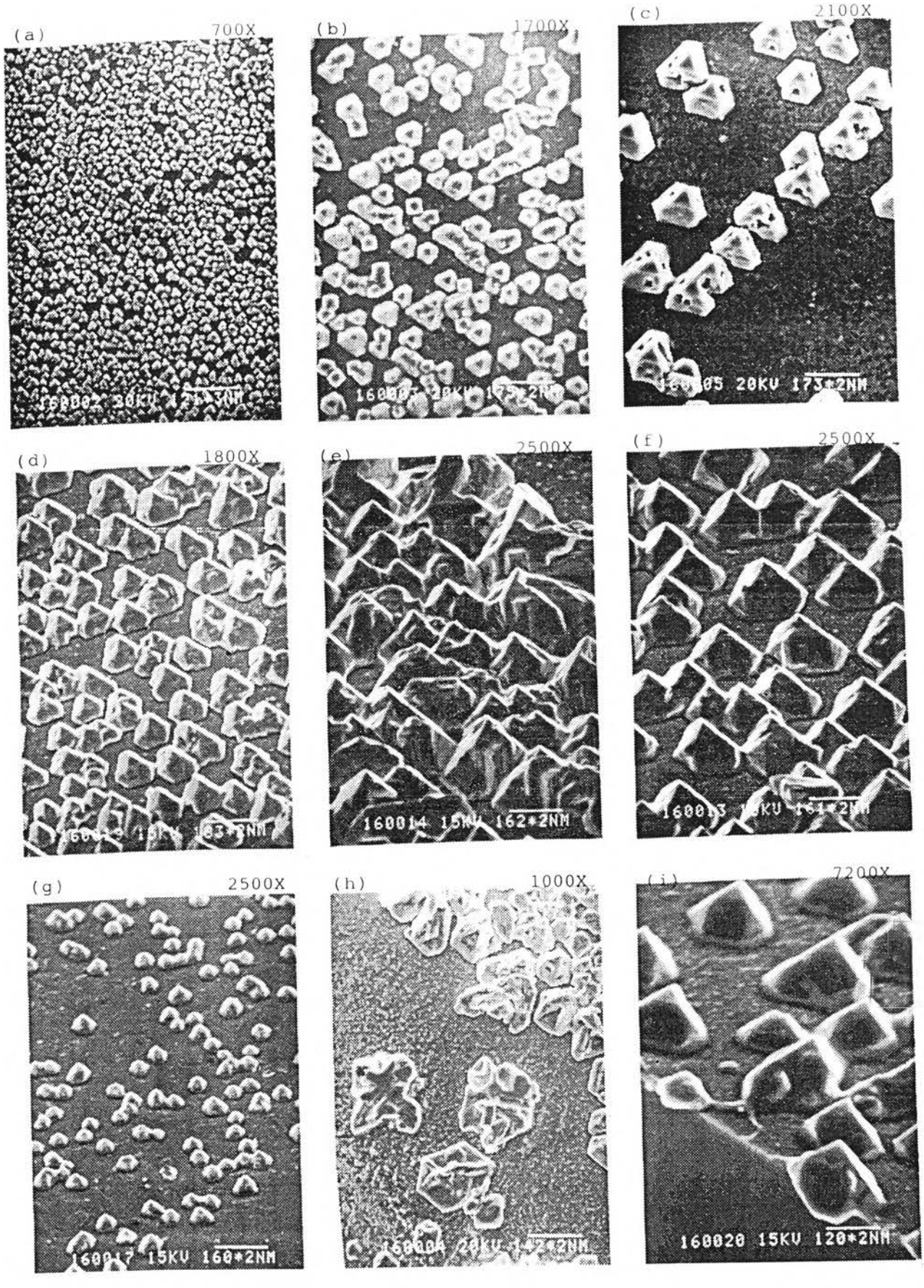

Fig.31 Scanning electron image at various magnification at some areas show the islets of Sn and the etched surface of InSb of method II growth of sample no. 16.

The morphologies of the results are shown in Fig. 29, 30, and 31 for sample 14, 15, and 16 respectively. Although some indication of the benefits of slower etching rate (lower T) in promoting more uniform site density over the wafer area, clear-cut correltion between the growth quality and a single parameter (one of T,t) could not be stated.

It is concluded that this "method 1" which is the easiest to set up in comparison with the other "methods" described in Chapter II does not yield reproducible result. Even different areas on the same sample yields different results, as shown in Fig. 29, frames d,e, and f at approximately the same magnification.

Samples from "Method 2" ($T >> T_s$ at immersion, then $T < T_s$)

As discussed in Chapter II high immersion temperature causes too rapid etching and results in rough surface features. Large growth features however make it convenient for EPMA mapping of the composition of the growth. Fig. 32 shows in a) scanning-electron beam image of a group of islet growths, in b) EPMA/WDS mapping of In while in c) mapping of Sn. This confirms that Sn is on top of the In layer (i.e. InSb) and, since the edges of the islets are aligned, that the growth is epitaxial.

We pursue no further study on the "method 2" samples and do not recommend this method for growing thin epitaxial film.

(a)

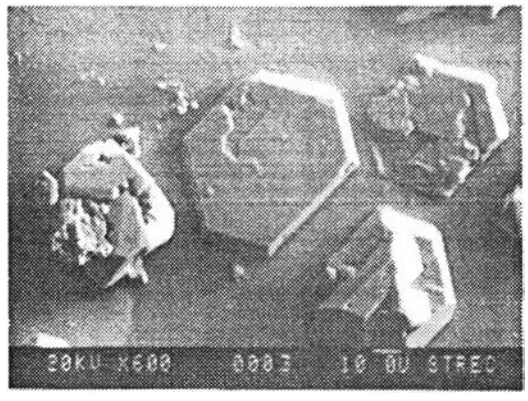

(b)

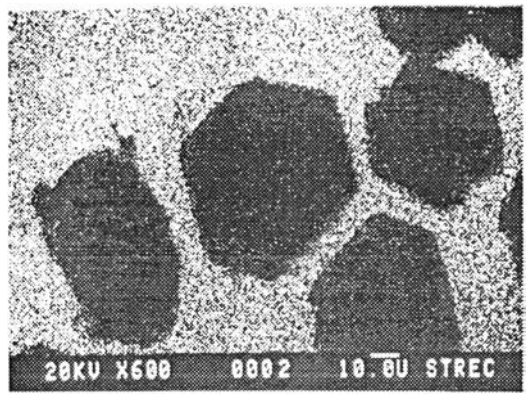

(c)

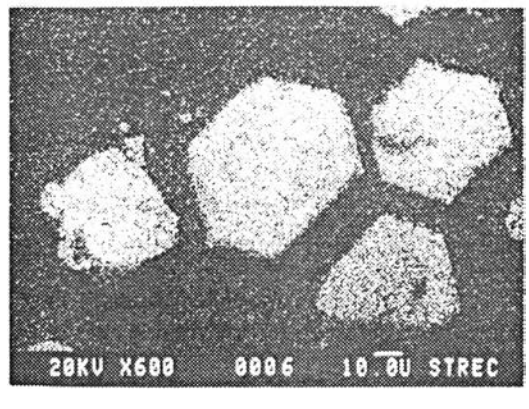

Fig.32 Scanning electron image of sample no.5
in (a) shows the same oriented islet Sn edges.
(b) and (c) shos the In and Sn mapping respectively
of the same area in (a).

Samples from "Method 3" ($T > T_s$ at immersion, then $T < T_s$)

Fig. 33 and 34 show SEI picture and EPMA/WDS mapping at two magnification factors for sample 9, which was so thickly covered with Sn deposit (see Chapter II). Fig. 35 shows similar pictures as in Fig. 34 but for sample 10. Comparing the temperature profiles for the samples 9 and 10 in Fig. 15, sample 10 should represent the nucleation stage (T just get below T_s) for the growth on sample 9. Here in Fig. 35 spotty nucleation sites are observed; Sn deposits on the InSb substrate through pin holes in the oxide layer. (This pin-hole hypothesis would be supported as described below.)

Samples from "Method 4" ($T < T_s$ at immersion and further decreases)

Sample 11 (whose temperature profile for growth is shown in Fig. 16) is cleaved and the cross-section examined by SEI in Fig. 36 a, and by EPMA/WDS oxygen mapping in Fig. 36 b. The oxide layer thickness is a few microns. EPMA/WDS mapping of In, Sn and Sb in frames c, d, and e show the InSb/oxide interface position, except of course frame d for Sn which shows nothing.

Fig. 37 a shows SEM of a region on the sample 11. The demarcation between the portion that was dipped and that above the liquid is shown. Fig. 37 b, c, d are EPMA/WDS of In, Sn, and Sb respectively. To increase the Sn detection sensitivity and reduce the beam penetration the electron beam energy is reduced to 15 kV and the magnification increased, and the x-ray detector current is metered.

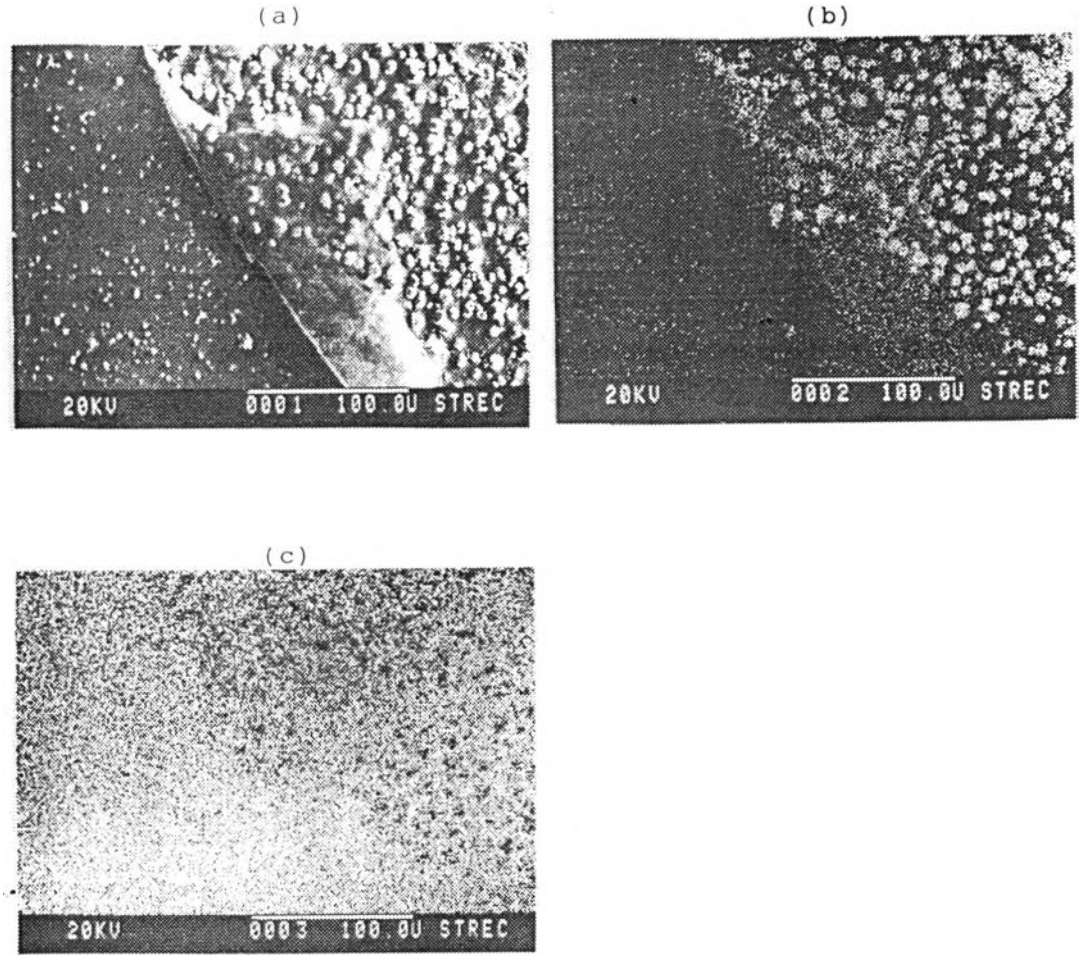

Fig.33 Scanning electron image of sample no.9 in (a) show the islet Sn on InSb. (b) and (c) shows the EPMA/WDS mapping of Sn and Sb respectively of the same area in (a).

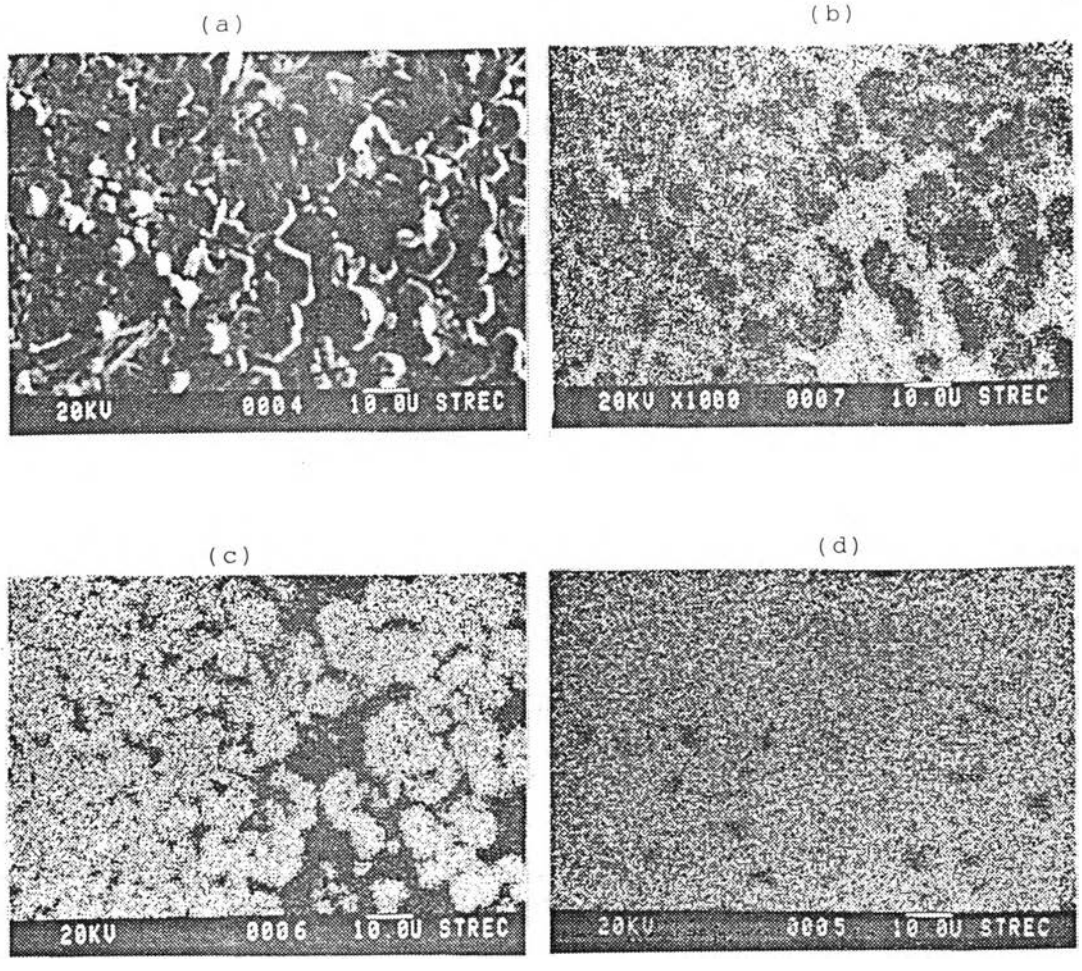

Fig.34. Scanning electron image of sample no.9
in (a) shows the dense islet Sn on InSb.
(b), (c) and (d) show the EPMA/WDS mapping of In,
Sn, and (d) respectively of the same area in (a).

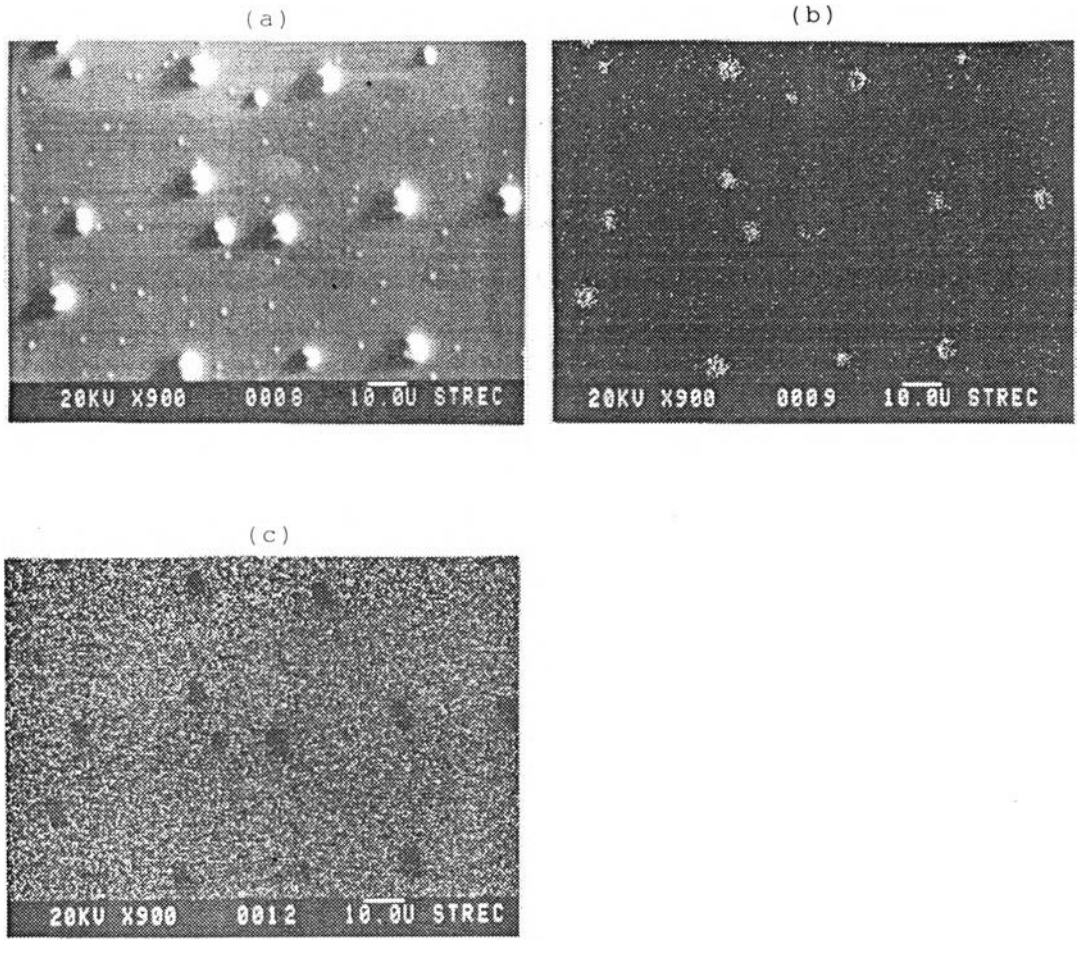

Fig.35. Scanning electron image of sample no.10
in (a) shows the initial state growth of islet
Sn on InSb. (b) and (c) show the EPMA/WDS
mapping of Sn and In respectively of the same
area in (a).

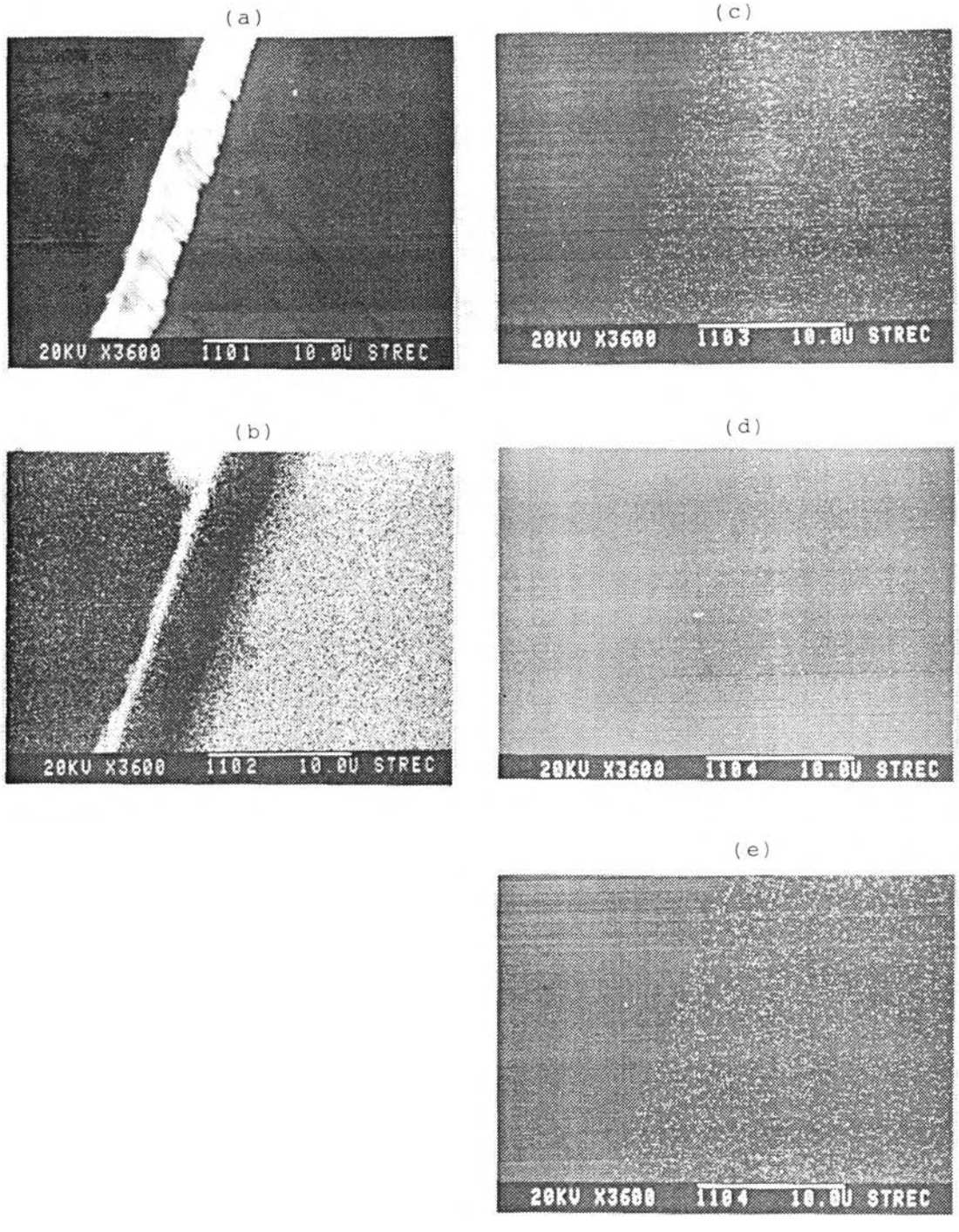

Fig.36 a) Scanning electron beam image of the oxide layer; the substrate body in the region to the right of the band. b) - e) EPMA/WDS data respectively for O, In, Sn, and Sb over the sample place as in a)

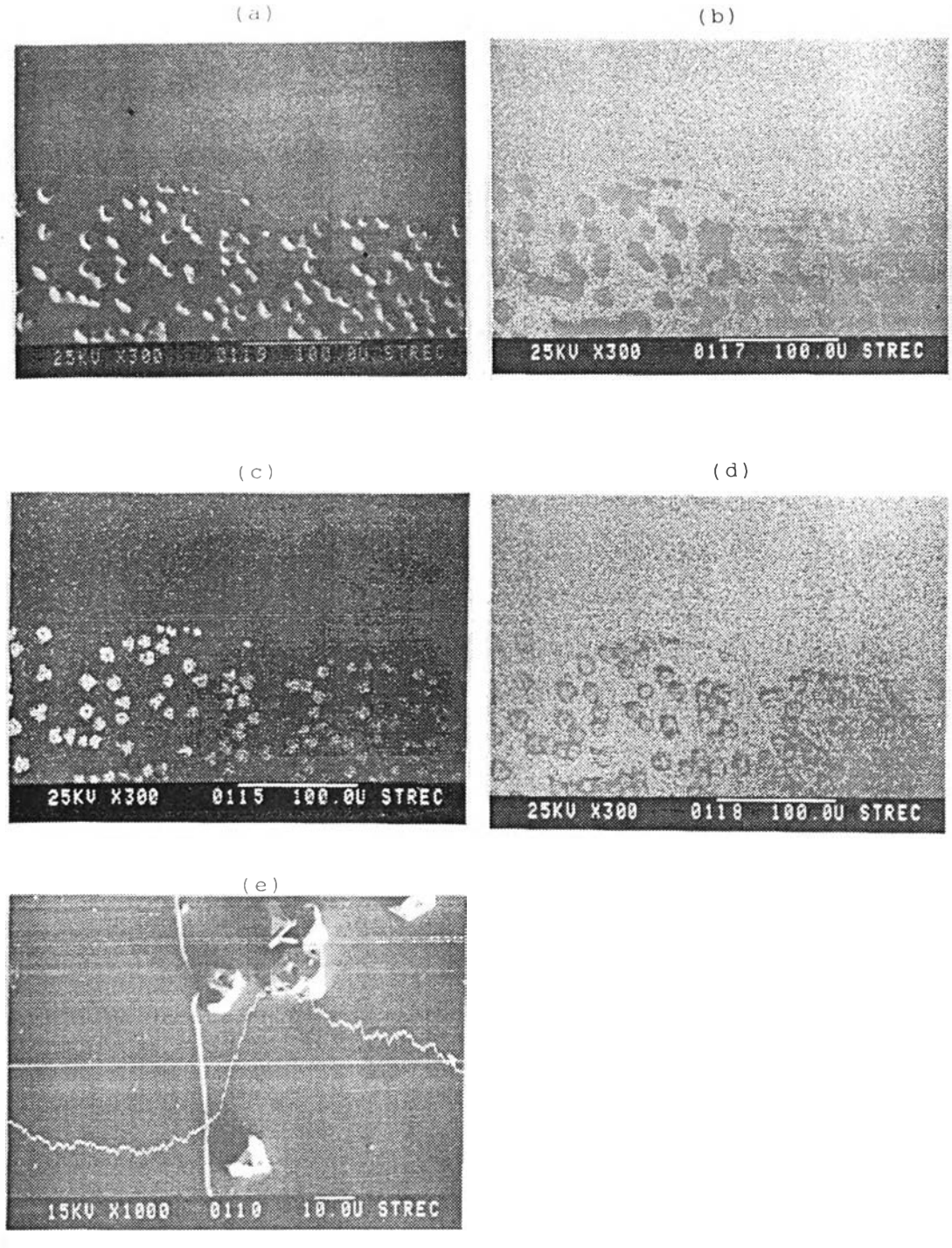

Fig.37 a)SEM scan showing growth of islet below the dip level(sample 11, b) - d) Low magnification EPMA/WDS scan of the same region as in a). c) (Sample rotated 90°, dipped region to the right, higher magnification.) Showing low source energy (15 kV instead of 25 kV) EPMA/WDS integrated signal plotted as jagged curve indicating presence of Sn. The straight horizontal line indicates the scanned positions.

Table 5 Current (picoamps) from x-ray detector of WDS by spotting electron beam on the cleaved cross-section sample starting from the surface into the substrate (1 μ in each step).

Distance from the surface into the substrate (μ)	0	1	2	3	4	5	6	7	8
Sample No. 11	.04	.08	.04	.02	.02	.02	.1	.1	
12	0	.13	.13	.08	.05	.05	.05		
13	.02	.10	.15	.46	.42	.36	.30	.30	.30
14	0	.10	.10	.08	.06	.04	.04	.04	
15	.04	.58	.30	.24	.24	.24			
16	.02	.28	.24	.22	.22	.22			

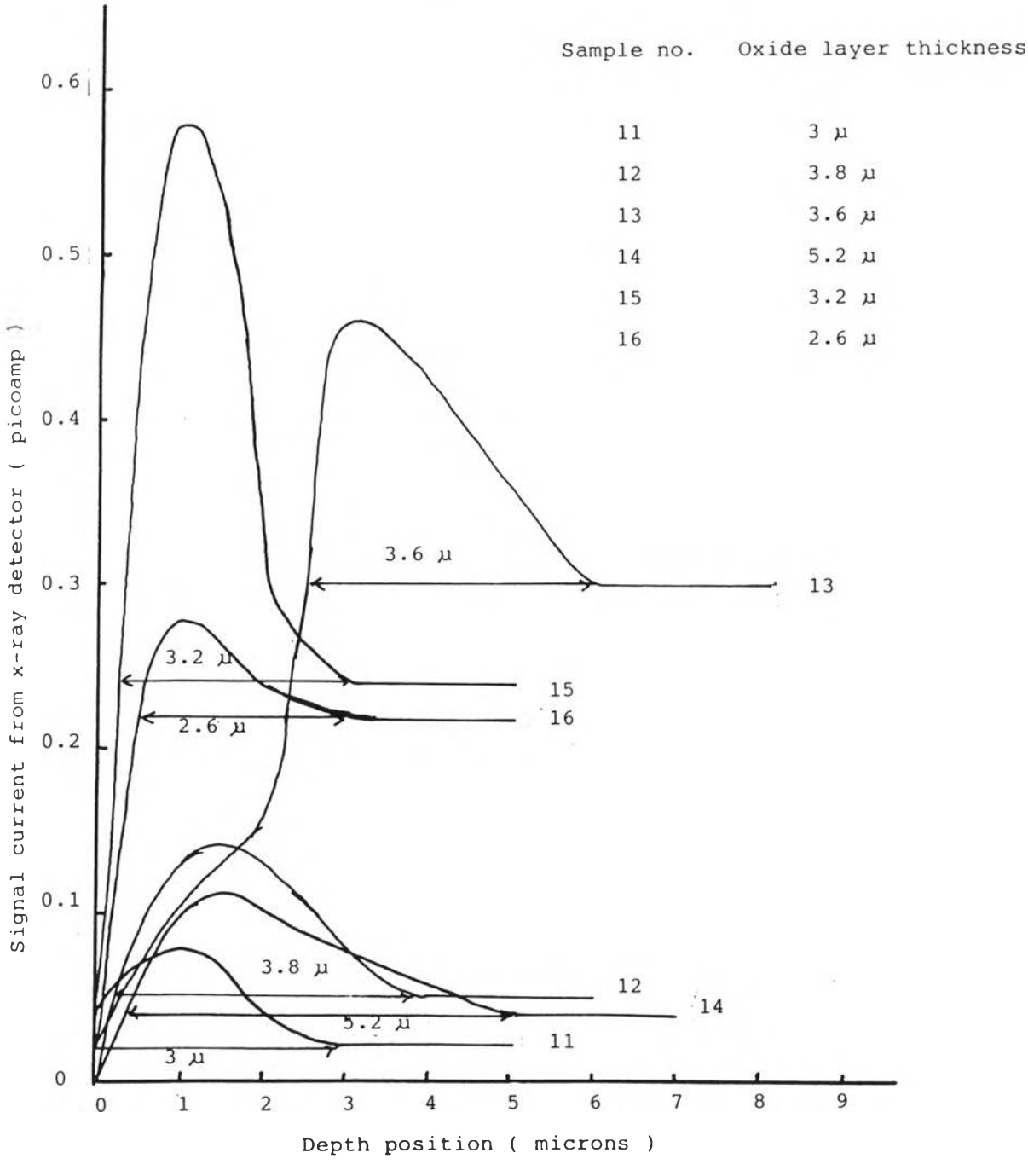

Fig. 38 The x- ray detector current vs depth position from the surface into the substrate.

The plot of current (corresponding to Sn amount) vs scan position is plotted as a jugged curve in Fig. 37 e; the horizontal straight line indicates the path on the sample which is photographed from SEM mapping.

Existence of the oxide layer is established over many epitaxy samples by using the EPMA/WDS technique for O instead of for Sn as described for Fig. 37 e, above. the x-ray detector current is measured as a function along the cleaved cross-section as in Fig. 36 e. The current is measured as various distance starting from the surface into the substrate. The results are tabulated in Table 5, and plotted in Fig. 38. In this figure the current vs depth position shows a peak and then returns to a new plateau not at the same level as the initial zero level. The new "zero" level is non-zero due to the presence of oxygen on the cleaved surface. The surface oxygen contamination level differs sample to sample.

X-Ray Back Reflection to Follow the Phase Change of Grey Tin.

The experimental methods used in obtaining diffraction patterns will be described in this section. Here we are concerned with the Laue method (31) only, especially the back reflection method applicable to this work. Ordinarily, the presence of strong characteristic x-ray component, such as CuK_{α} (1.540 Å in wavelength) in the radiation used, does not complicate the diffraction pattern in any way or introduce difficulties in its interpretation. Such a component will only be reflected if a set of planes in the crystals happens to be oriented in just such a way that the Bragg law is

satisfied for that component, and then the only effect will be formation of a Laue spot of exceptionally high intensity.

The specimen used in the Laue method is a single crystal. Laue spots are often formed by overlapping reflections of different orders. For example, the 100, 200, 300,... reflections are all parallel. The first-order reflection is made up of radiation of wavelength λ , the second-order of $\lambda/2$, the third-order of $\lambda/3$, etc., down to λ_{SWL} , the short-wavelength limit of the continuous spectrum.

The position of any Laue spot is unaltered by a change in plane spacing, since the only effect of such a change is to alter the wavelength of the diffracted beam. It follows that two crystals of the same orientation and crystal structure, but of different lattice parameters, will produce idential Laue patterns. In this experiment, the diffracted beam from α-Sn and InSb are at the same position of Laue patterns because the crystal structure of α -Sn and InSb are the same face centered cubic and the lattice parameters are nearly the same size.

This section will describe a technique which was developed to follow the transformation of the cubic α -Sn phase, laid islet structure on (111)B face of an indium antimonide single crystal, to a polycrystalline form of the tetragonal white tin phase. The grey-white phase transformation was observed to occur at around 60 $^{\circ}$C, and the white-phase was found to be retained during cooling to room temperature (26 $^{\circ}$C). This phase change is important in the epitaxial

α-Sn since the transformation is likely to destroy the single crystal nature of the epitaxial α-Sn.(32)

The work was carried out on a Unicam Goniometer incorporating a specially designed heating stage capable of heating the sample up to approximately 100 °C. The Unicam Goniometer with the heating stage is shown in Fig. 39. The main body of the stage is made of copper and has a rod heater inserted in its body, the currrent to the heater being controlled by a variac. At a variac setting the temperature would rise and eventually reaches an equilibrium value. The temperature measurement was done using chromel/alumel thermocouples or mercury thermometer which was situated in closest to the sample. The sample holder made from bakelite slots into the groove of the heating stage. The sample was held on the sample holder with a clay adhesive and gallium-indium alloy was used for thermal contact to the heating stage.

Initially, the technique to be employed on the (111)B face InSb at room temperature, the idea was to take for reference the three-fold symmetry back reflection photograph from the face centered cubic crystal structure and compare with the epitaxial α -Sn on InSb sample which was heated to various temperatures up to approximately 100 °C. After allowing the temperature to reach equilibrium, taking x-ray photographs with 2-8 hours exposure time. The 30 KV 25 mA power setting was used.

In this work, the α -Sn is only in islet crystal form, the back reflection spots from the islet crystal misoriented a little from

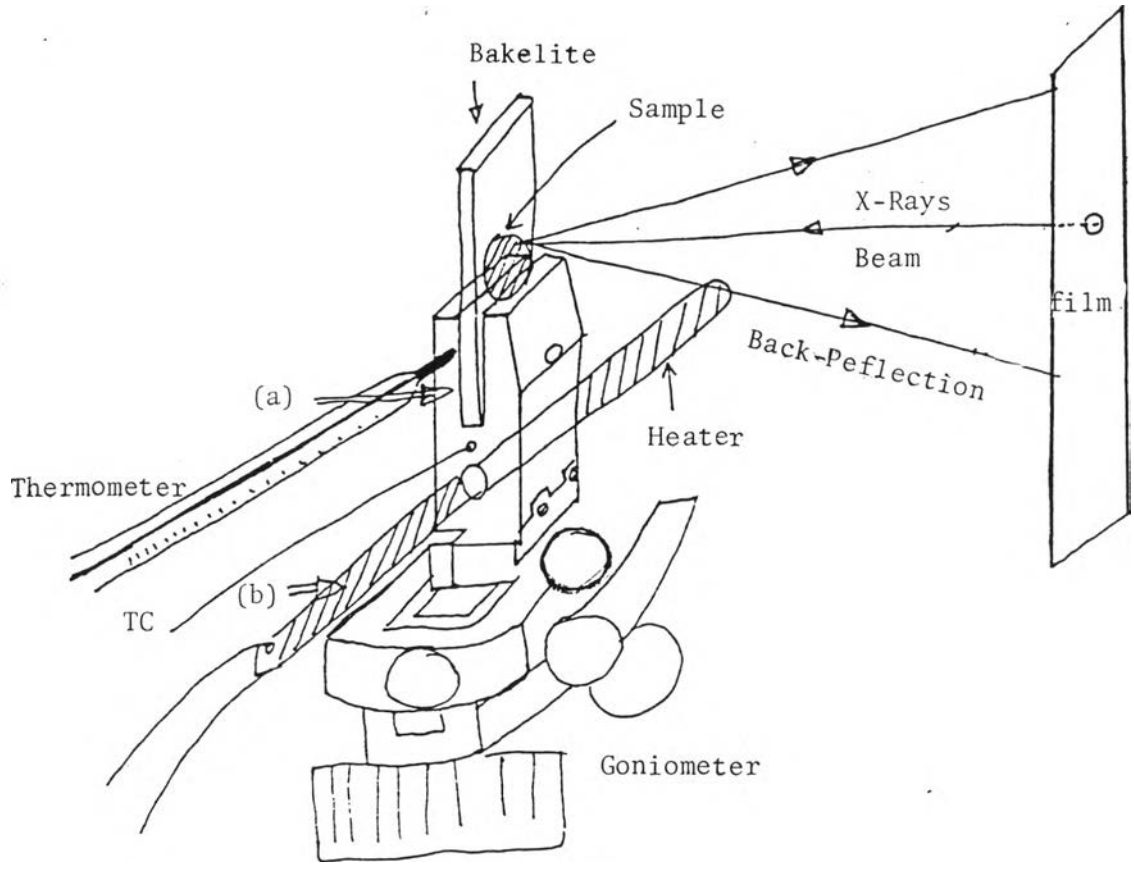

Fig.39 Sample heating stage showing:

(a) copper heating stage

(b) solder rod heater.

The stage is seen clamped in position on a Goniometer.

(111) face will give a partial Debye ring. When the α-Sn/InSb was heated up to approximately 60 °C, that partial Debye ring diameter was increased. We can identify that the partial Debye ring from (642) α-Sn plane was changed to the partial Debye ring from (541) β-Sn plane. The detailed calculation will be discussed in the next section.

Experimental Results and Discussion - X-Ray Back Reflection Experiment.

The x-ray back reflection technique discussed above was applied to the Sn on InSb samples. In as much as the beam diameter is much larger than the size of a single Sn islet, an area of dense population of epitaxial islets is selected. The x-ray result is thus of the aligned multiple grains or islets.

Figure 40 a and 40 b show the results for room temperature and at 60-70 °C respectively. As explained in the previous section the pictures must be superimposed to align the major Debye rings (belonging to the InSb substrate) to correct for the experimental (relative position) misalignment between the two experiments, so that the center of all Debye rings can be located in each picture. Based on these centers, the partial Debye ring indicated in Fig. 40 a is identified as that from the (642) plane of the α-Sn and that in Fig. 40 b is from the (541) plane of β-Sn. This is based on the following analysis :

Reffering to Fig. 41.

$$\tan (180^\circ - 2\theta) = r/D \qquad (3.3)$$

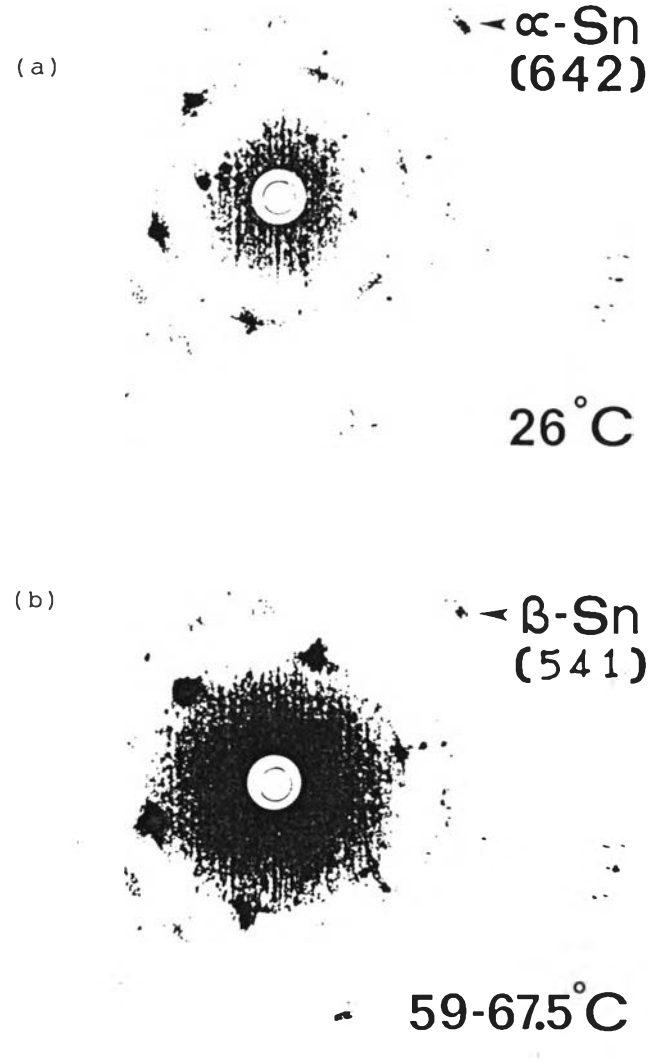

Fig.40 X-ray back reflection of islet Sn on InSb to follow the phase change from $\alpha \rightarrow \beta$ (a) showed partial Debye ring from diffracted plane (642) of α-phase. (b) showed partial Debye ring from diffracted plane (541) of β-phase.

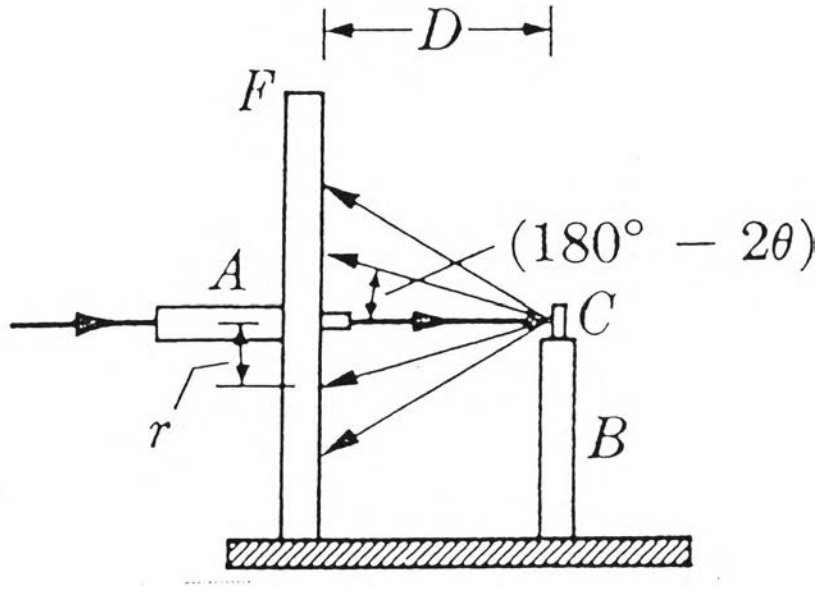

Fig.41 Back-reflection Laue camera (schematic). A is the collimator. C is the specimen supported on the holder B. F is the light-tight film holder (cassette). r is the distance of spot from center of film. D is specimen-to-film distance (usually 3 cm).

Table 6 Pattern of α-Sn (back-reflection)

d (Å)	I/I_1	hkl	$\sin\theta = 1.5405/2d$	θ	V = 2D tan (180°-2θ), D=3 = Debye ring dia.(cm)
0.9087	7	711	0.8476	57.9558	12.35
0.8671	13	642	0.8883	62.6611	8.47
0.8450	12	731	0.9115	65.7188	6.80
0.8111	-	800	0.9496	71.7331	4.44

Table 7 Pattern of β-Sn (back-reflection)

d (Å)	I/I_1	hkl	$\sin\theta = 1.5405/2d$	θ	V = 2D tan (180°-2θ), D=3 = Debye ring dia.(cm)
0.8868	4	323	0.8686	60.2932	10.15
0.8755	2	541	0.8798	61.6162	9.16
0.8485	4	413	0.9078	65.2001	7.05
0.8466	4	532	0.9098	65.4799	6.91

Defining V as the Debye ring diameter, we write (3.3) as

$$V = 2D \tan (180^{\circ} - 2\theta) \qquad (3.4)$$

The (hkl) plane separation distance d is related to the cubic side dimension a as

$$1/d^2 = (h^2 + k^2 + l^2) / a^2 \qquad (3.5)$$

while for a tetragonal structure of side parameters a and c

$$1/d^2 = (h^2 + k^2)/ a^2 + l^2 / c^2 \qquad (3.6)$$

We investigate some hkl combinations which would yield the Debye ring diameter of interest. (Note h,k,l must be either all odd or all even)

Table 6(33) shows the calculation of V for a few combinations of h,k,l of the α-Sn structure for λ = 1.5405 $\mathring{A}$ (CuK_{α}). The relative intensity ratio, I/I_1 is also shown on the table for spot brightness identification. The d values are from eq.(3.5).

Table 7(33) shows the V values for a few combinations of h,k,l of the β-Sn structure for λ = 1.5405 $\mathring{A}$. Inspection of the two tables show that the two partial Debye rings shown in Fig. 40 are indeed identifiable as (642) α-Sn and (541) β-Sn.

The x-ray back scattering result as described above therefore verifies that α-Sn from our epitaxy experiment is stable up to $\simeq$ 60 $^{\circ}$C beyond which it reverts to the β-phase.